JOURNAL OF AIRCRAFT
Vol. 32, No. 6, November–December 1995

Double-Delta-Wing Aerodynamics for Pitching Motions With and Without Sideslip

Deborah S. Grismer*
U.S. Air Force Wright Laboratory, Wright–Patterson Air Force Base, Ohio 45433-7531
and
Robert C. Nelson†
University of Notre Dame, Notre Dame, Indiana 46556-5684

Subsonic aerodynamic experiments, both with and without sideslip, were performed on a strake/wing planform for both static and dynamic conditions. The strake sweep, wing sweep, and strake-to-wing fineness ratio for the model was 80 deg/60 deg/0.6. Flow visualization information was obtained by marking the strake and wing vortices with smoke in order to determine the state of the vortices (i.e., existence, pre- or postbreakdown). Five-component force and moment data was also taken. Both the flow visualization and the force and moment information were obtained for the model at static angles of attack, as well as for the model undergoing sinusoidal pitching motions. The minimum and maximum angles of attack of the motions were varied. Also varied were the reduced frequencies of the motions. The combined information obtained from the flow visualization and force experiments was used to explain some of the dynamic effects observed for the double delta wing.

Nomenclature

b = maximum wingspan
C = test section cross-sectional area
C_N = normal force coefficient, NF/$q_\infty S$
C_l = rolling moment coefficient, RM/$q_\infty Sb$
c = root (centerline) chord length
f = frequency of the sinusoidal motion
k = reduced frequency, $2\pi fc/V_\infty$
k_f = fitness ratio, x_s/c
NF = normal force
q_∞ = dynamic pressure
Re = Reynolds number, $\rho_\infty V_\infty c/\mu_\infty$
RF = rolling force
S = planform area
S_f = projected frontal area, $S \sin(\alpha)$
s = local semispan
V_∞ = freestream velocity
x = axial wing coordinate from apex of model
y = spanwise wing coordinate from centerline of model (positive on the starboard side)
z = vertical wing coordinate above surface of model
α = angle of attack, $\tan^{-1}(\tan \alpha_Y/\cos \beta)$
β = angle of sideslip
Λ = leading-edge sweep angle
Λ_e = effective leading-edge sweep angle, $\Lambda \pm \beta$
μ_∞ = absolute viscosity of air
ρ_∞ = density of air

Subscripts
s = strake section
w = wing section aft of strake
Y = the yoke

Received Sept. 14, 1994; revision received May 10, 1995; accepted for publication May 20, 1995.

*Captain, Flight Dynamics Directorate, Building 146, Room 305, 2210 Eighth Street, Suite 21. Student Member AIAA.

†Professor, Department of Aerospace and Mechanical Engineering, Hessert Center for Aerospace Research, Building 66, Room 106. Associate Fellow AIAA.

Introduction

A DOUBLE delta wing is a planform that incorporates two distinct leading-edge sweep angles. The first part of a double delta wing model, the strake, has a significantly higher sweep angle than the aft portion of the model, the main wing. The double delta planform is similar to the planform used for several military fighter aircraft, supersonic transport aircraft, as well as the planform proposed for the National Aerospace Plane. The double delta wing has been shown to have better aerodynamic performance than a simple delta wing having the same sweep as the main wing of the double delta and a comparable area. The improved aerodynamic performance, especially at the higher angles of attack, is due to the interaction of the vortices created by the strake and main wing. The strake vortices tend to stabilize the main wing vortices and delay vortex breakdown to a higher angle of attack than would be possible for a simple delta wing of the same sweep as the main wing. The interaction of the strake and wing vortices also produces an increase in the nonlinear vortex lift for the double delta wing.

There have been a number of research efforts to examine the performance of double delta wings.[1–6] There have been much fewer studies that examined the performance of delta and double delta wings in sideslip.[7–10] In sideslip, each side of the wing experiences an effective change in sweep angle. The side leading into the flow will see an effective decrease in sweep angle, whereas the side trailing will see an effective increase in sweep angle. On a double delta wing this can result in some very complex interactions. The decrease in effective sweep will cause stronger vortices, but it will also increase the likelihood of vortex breakdown occurring over the wing. The side that experiences an increase in effective sweep will have weaker vortices, but a greater possibility of strong interaction between the strake and wing vortex. Several observations and conclusions about double delta wings in static positions of sideslip were discussed in previous papers.[11,12]

In the past several years there has been an interest in what has been termed "supermaneuverability." This involves dynamic flight maneuvers in which an aircraft moves into the high angle-of-attack range. These types of flight maneuvers usually occur at relatively low speeds. The interest in unsteady aerodynamics, in general, has increased in recent years. Due to the flow unsteadiness during dynamic maneuvers, the aero-

dynamic behavior of a wing is significantly more complicated than for the static condition. The effects from these dynamic maneuvers may be either beneficial or detrimental.

A few studies have examined the performance of delta wings undergoing dynamic pitching motions.[13-21] There have been very few studies, however, that looked into the aerodynamic effects of double delta wings undergoing dynamic pitching maneuvers.[22-24] These dynamic studies have noted that for these wings there are flowfield differences between the upstroke and downstroke of a particular motion. The vortex breakdown position has been seen to lag the static position. These differences between the upstroke and the downstroke are the cause of the hysteresis loops that have been observed in the forces and moments. The size of these hysteresis loops depends not only on the model geometry, but also upon the precise motion of the maneuver. There is, therefore, a need for more aerodynamic and flow visualization data on double delta wings undergoing dynamic maneuvers, especially at nonzero sideslip, to aid in the understanding of the complicated flowfield that results under these conditions.

This study presents flow visualization and force information for an 80 deg/60 deg/0.6 double delta model at fixed angles of attack and for the model undergoing sinusoidal pitching motions. These tests were performed for the model mounted to the pitching apparatus at zero and nonzero sideslip angles. Static measurements were made and discussed in the previously mentioned work and so they will not be the focus of this article. Data obtained from the model being driven dynamically, through sinusoidal pitching motions, will be the primary focus. Some static data is presented, but it is primarily meant to serve as a basis for comparison with the dynamic results.

Experimental Apparatus

The experiments described in this article were conducted in an indraft low-speed wind tunnel. The results discussed in this article are for an 80 deg/60 deg/0.6 double delta wing. The same model was used for all of the tests. A planview drawing of this model is shown in Fig. 1. The strake sweep angle Λ_s and the wing sweep angle Λ_w are 80 and 60 deg, respectively. The ratio of the strake chord to total chord is 0.6. The model was a 1.27-cm- (0.5-in.-) thick flat plate with sharp upper-surface leading edges resulting from a 45-deg underside bevel. There was no bevel on the trailing edge.

Sideslip and the model coordinate system are also defined in Fig. 1. For a negative sideslip angle, the leading edge of the port side of the model experiences a reduction in the effective sweep angle and the leading edge on the starboard side sees an effective increase in sweep angle. With the wing oriented at a negative sideslip angle, as shown in Fig. 1, the port side of the model will be referred to as the windward side and the starboard side will be referred to as the leeward side. These are the terms that will be used in discussions pertaining to the effects of variations in sideslip angle. These terms are not to be confused with windward, referring to the underside of the wing, and leeward, referring to the region above the wing, for positive angles of attack.

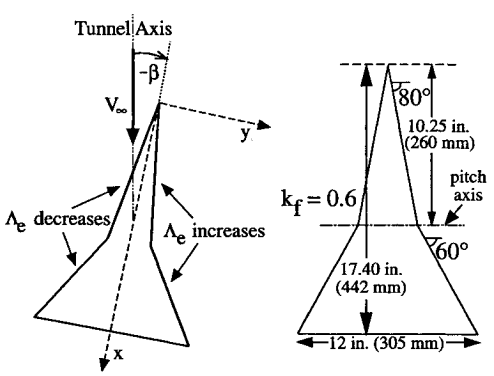

Fig. 1 Coordinate system and geometry for the 80 deg/60 deg/0.6 double delta wing.

At a fixed sideslip angle, the double delta wing was pitched through various sine wave motions. The minimum and maximum angles of attack of the motions were varied. The model was driven through ranges of motion from a minimum of α = 30–40 deg through a maximum of α = 0–60 deg. At a fixed angle of attack range, α = 0–40 deg, the model was also pitched at different rates, thereby varying the reduced frequency. Tests were performed for values of k from 0 (static) through 0.08, in incremental values of 0.02. Flow visualization experiments were performed for most of these motions with the model at sideslip angles of β = 0 and −6 deg. Force and moment measurements were taken for these motions with β = 0, −3, and −6 deg.

A pitching apparatus was constructed to vary the angle of attack of the model, either statically or dynamically, at fixed sideslip angles. All experimentation was performed with this apparatus. A sketch of the apparatus comprising this pitching system is shown in Fig. 2. This new system employed a motion control system previously developed at the University of Notre Dame by Arena.[25] The model is mounted via a rear sting attached to a yoke-type of pitching apparatus similar to that used by Jarrah.[26] To mount the model at different sideslip angles, a different back horizontal bar was used. The rear sting was offset from the horizontal centerline of the bar for nonzero sideslip angles. This ensured that the pivot point of the model remained at the horizontal centerline of the test section. The model was pitched about a pivot line that intersected the axial location of the strake/wing juncture at the model's centerline. For β = 0 deg, the pitch axis is shown in Fig. 1. For nonzero sideslip angles, the angle of attack of the yoke does not equal the angle of attack of the model. Knowing the angle of attack of the yoke and the sideslip angle, the angle of attack of the model can be computed according to the equation listed in the Nomenclature.

Flow visualization was undertaken, both with the model at static positions and with the model in motion, in order to better understand the role of the leading-edge vortices and their effect on the model performance. The leading-edge vortices were made visible with smoke particles and visual images were recorded on videotape. The smoke production involved vaporizing titanium tetrachloride ($TiCl_4$) in a stream of nitrogen gas. The resulting $TiCl_4$/nitrogen mixture came into contact with airborne water vapor immediately upon leaving the model ports that were located near the strake apex and the strake/wing juncture. The reaction proceeded quickly enough

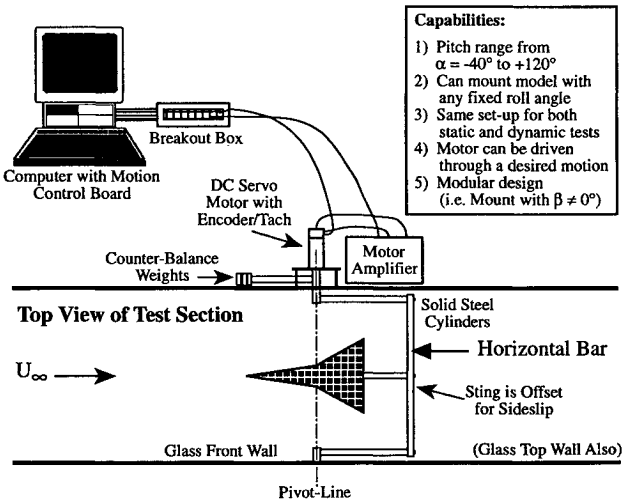

Fig. 2 Schematic of the pitching apparatus.

that the products were immediately visible, yielding an effect much like that of dye injection in water. A detailed discussion of this flow visualization technique is presented by Visser et al.[27]

The five-component force and moment data was acquired from an internal five-component force balance. The signals from the force balance were passed through external amplifiers, then through low-pass filters, with a cutoff frequency of 4.8 kHz, to reduce the hf noise components generated by the motor amplifier. Each channel of data was acquired simultaneously. Static force data was acquired at a sampling rate of 500 samples/s for 5 s. Therefore, the static force data at a given model position was an average of 2500 samples. The force data acquired during dynamic motions was sampled at a rate of 100 samples/s. Since the fastest rate through which the model was pitched was 0.727 Hz, this sampling rate was adequate. It still captured the small oscillations, or vibrations, the model underwent throughout the large pitching motions. The dynamic data that will be discussed in this article, shown for one cycle of motion, is an ensemble average of at least 60 cycles.

Flow visualization tests were conducted at a Reynolds number based on the model centerline chord of 1×10^5. Flow visualization of vortical structures has shown the basic flow characteristics to exist over a wide range of Reynolds numbers. Thompson[28] has shown small displacements in the vortex trajectories with changes in Reynolds number for Reynolds numbers under 1×10^5. However O'Neil et al.[29] studied delta wings and found the location of vortex breakdown as well as surface pressure and force results to be virtually independent of Reynolds number for higher Reynolds numbers. They found that for flat plate wings the leading-edge geometry played a much more significant role in determining the location of vortex breakdown. Because this model had sharp leading edges, separation was fixed at the leading edge. Based on the leading-edge geometry and the O'Neil et al. study, which focused on Reynolds numbers over 1×10^5, it was decided that the force tests could be performed at a higher Reynolds number and the results of these tests could be compared with the flow visualization results. Therefore, the force and moment data were obtained at a Reynolds number of 7.25×10^5.

The test section used for these experiments had a 61×61 cm (2×2 ft) cross section. The total model planform area was 484 cm^2 (75.1 in.^{2}). The maximum span-to-tunnel-width ratio was 0.5. At $\alpha = 90$ deg this model would produce a blockage ratio S_f/C of 13.0%. However, at $\alpha = 60$ deg S_f/C reduces to 11.3% and at $\alpha = 40$ deg it drops to 8.4%. The effects of wake blockage for this model were investigated. The method of Pass,[30] an empirical alteration of the Maskell[31,32] approach, applied to a series of delta and trapezoidal wings, was attempted for the double delta wing of this study. These blockage effects on the force coefficients were discussed in a previous paper by Grismer et al.[11] This wake blockage correction increases the dynamic pressure, thereby reducing the absolute value of the nondimensionalized force and moment coefficients. Applying this technique, these coefficients were reduced by 11.3% at $\alpha = 40$ deg and by 8.1% at $\alpha = 30$ deg.

The Pass technique does not account for blockage from the U-shaped yoke, the model pitching structure, and sting. At $\alpha = 90$ deg the yoke by itself would produce a blockage ratio S_{f_Y}/C of 6.7%. At $\alpha = 60$ deg S_{f_Y}/C reduces to 6.2% and at $\alpha = 40$ deg it drops to 5.3%. Therefore, accounting for not only the model, but also the yoke, the total blockage ratios at $\alpha = 90$, 60, and 40 deg were 19.7, 17.5, and 13.7%, respectively. The largest angle of attack through which the model was pitched was $\alpha = 60$ deg, but for all of the other motions, the maximum angle of attack achieved was $\alpha = 40$ deg.

Because neither this correction technique nor other examined techniques took the yoke or sideslip into account along with the dynamic behavior of the flow, and because they were not developed specifically for double delta wings and did not appear to apply well to the double delta wing, it was decided that it would be better to present the experimental data without any attempt at applying a blockage technique in this article. The absolute magnitude of data that will be presented is expected to be reduced slightly by accounting for the blockage, but the overall trends that will be discussed in this article for motion variations remain the same.

Discussion of Results

Effect of the Pitching System Support

Using a yoke-type pitching mechanism, the concern arose over whether the back horizontal bar, shown in Fig. 2, would cause interference with the double-delta-wing flowfield. A lightweight, symmetric fairing was constructed to fit over the bar so that it was free to move as the model was pitched, thereby keeping a horizontal orientation relative to the tunnel floor during testing. This fairing served to streamline the flow over the bar, thereby keeping the wake from the bar with the fairing confined to a small region in hopes of not interfering with the double-delta-wing flowfield. Flow visualization as well as both static and dynamic force tests were performed with and without the fairing over the bar, and the results from the two configurations were compared.

First, flow visualization was performed for the two configurations using kerosene smoke to provide a qualitative examination of the two flowfields. A comparison of the flowfields revealed no obvious interference from the bar for either configuration. Second, force measurements were made for the two configurations to get a quantitative measurement of possible differences. A static pitch-up and pitch-down force test was performed, as well as a dynamic test of the model undergoing a sinusoidal pitching motion. Figures 3a and 3b show the normal force coefficient for both the static and dynamic conditions, respectively, each with the fairing and without it. Overall, both the static and dynamic tests were relatively consistent between the two configurations. Note that for the static case, shown in Fig. 3a, a small static hysteresis was observed for the bar alone, but such a hysteresis was not observed for the fairing configuration. A plot of the normal force coefficient for the dynamic case, shown in Fig. 3b, has arrows to indicate the pitching direction. The dynamic case yields a clockwise hysteresis in the normal force coefficient. During a portion of the upstroke, the normal force coefficient yields a value larger than the static case, and during a portion of the downstroke the normal force coefficient yields a value smaller than the static case. This behavior has been found to be typical for delta wings undergoing pitching maneuvers.[13,15,16]

For both the static and dynamic case the agreement is good between the two through $\alpha = 35$ deg, but at higher angle of attack the bar-alone C_N is 3% lower than the fairing-on data. For the dynamic case the difference is almost within the small oscillations in the data. These oscillations are caused by vibrations of the model. Such oscillations were more noticeable at the higher angles of attack. The oscillations were observed for both the static and dynamic cases, but for static cases the data was acquired over a period of time and averaged to yield a single value. Therefore, from a qualitative analysis of the flow visualization, and from a quantitative analysis of the force data, it appeared that the back horizontal bar was not causing any significant interference with the double-delta-wing flowfield.

Effect of Sideslip on the Static Data

The normal force and rolling moment coefficients at static angles of attack are shown for three sideslip angles in Figs. 4 and 5, respectively. Clockwise static hysteresis loops are seen for both the normal force and rolling moment coefficients at each sideslip angle. For the normal force coefficient, shown in Fig. 4, with an increase in the magnitude of sideslip these

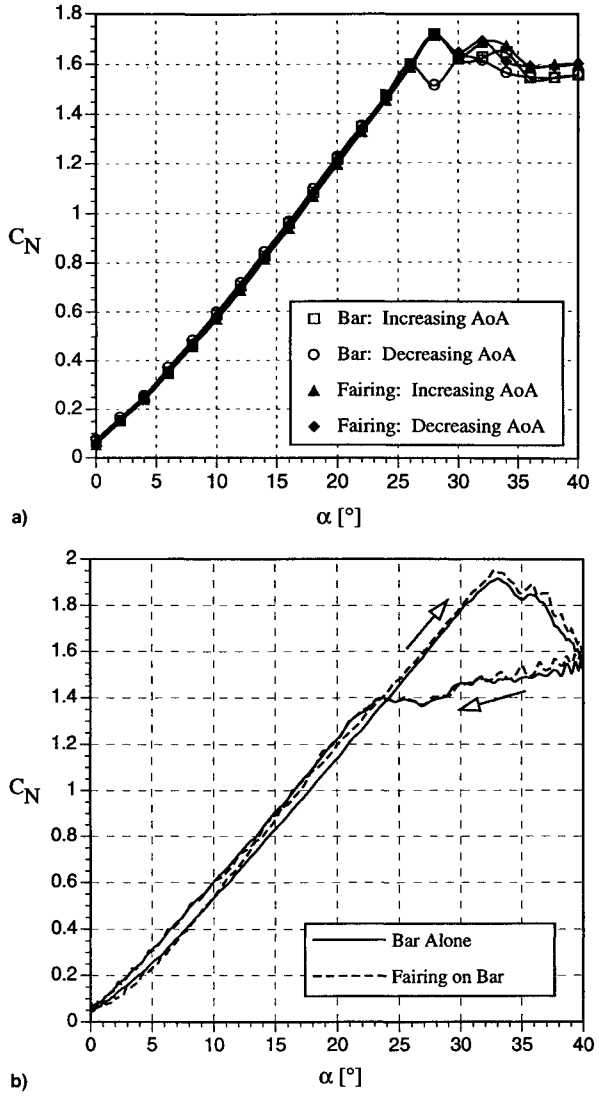

Fig. 3 a) Static normal force coefficient comparison for the horizontal bar alone and the fairing on the bar at $\beta = 0$ deg and b) dynamic ($k = 0.04$) normal force coefficient comparison with and without the fairing at $\beta = 0$ deg.

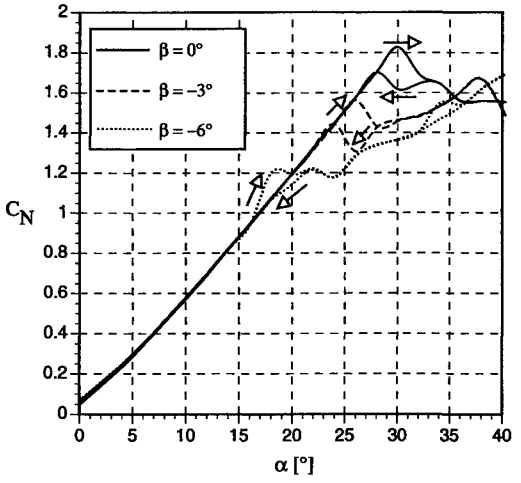

Fig. 4 Static normal force coefficient for three sideslip angles.

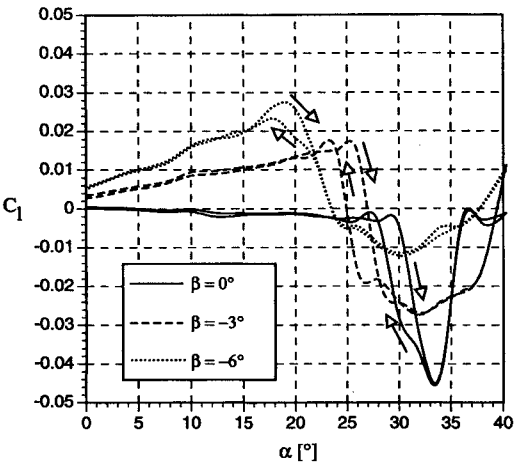

Fig. 5 Static rolling moment coefficient for three sideslip angles.

hysteresis loops occur at lower values of C_N and at lower angles of attack. For zero sideslip angle the peak hysteresis occurs at $\alpha = 30$ deg; at $\beta = -3$ deg the peak hysteresis occurs at $\alpha = 26$ deg; and at $\beta = -6$ deg it occurs at $\alpha = 18$ deg. Manor and Wentz,[33] who obtained static force and moment data for an 80 deg/65 deg/0.55 double delta wing, examined the aerodynamic effects of sideslip for angle-of-attack variations. They observed sideslip to cause a decrease in α_{stall} and an enhanced poststall lift recovery. For this planform, at each sideslip angle the normal force coefficient increases with angle of attack to the hysteresis region. At zero sideslip the C_N curve exhibits the most significant drop in value after the hysteresis occurs. For $\beta = -3$ deg, after the hysteresis region the normal force coefficient continues to increase with increasing angle of attack through approximately $\alpha = 37$ deg, where a drop in C_N is seen. For $\beta = -6$ deg, after the hysteresis region the normal force coefficient continues to increase with increasing angle of attack through $\alpha = 40$ deg. At $\alpha = 30$ deg, the largest value of C_N is observed for $\beta = 0$ deg and it decreases as the magnitude of sideslip is increased. This decrease in normal force with sideslip was also observed previously by Grismer et al.[11]

For the same angles of attack at which the static hysteresis loops occurred for the normal force coefficient, static hysteresis loops in the rolling moment were found. These hysteresis loops also have a clockwise orientation, as shown in Fig. 5. These curves show that for this range of sideslip angles, -6 deg $< \beta < 0$ deg, the model exhibits static roll stability for angles of attack up through $\alpha = 20$ deg. For higher angles of attack the model exhibits regions of static roll instability. At $\alpha = 30$ deg C_l is negative for each negative sideslip angle shown. These results support a previous study by Grismer et al.,[11] which examined the same double delta wing at fixed angles of attack with varying sideslip angle. The largest negative rolling moment is observed for the zero sideslip case. This case will be discussed later.

Effect of Varying the Reduced Frequency

Figures 6a and 6b show some flow visualization images taken at $\alpha = 36$ deg, $\beta = 0$ deg, and $k = 0.08$, during a sinusoidal oscillation from $\alpha = 0$–40 deg. Figure 6a was taken during the upstroke of the motion and Fig. 6b was taken during the downstroke. It is very apparent from these two images that the location of breakdown for the strake vortices was much farther from the apex for the upstroke than for the downstroke. Both Figs. 6a and 6b show asymmetric strake vortex breakdown. The implications of this asymmetry will be discussed later.

Figure 7 gives a graphical representation of how the location of vortex breakdown varies not only between the upstroke and the downstroke of a given motion, but also how it varies from one reduced frequency to another. In Fig. 7 the location of breakdown for the port strake vortex is shown for the static

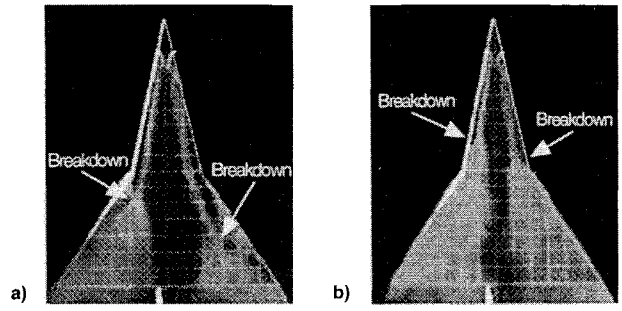

Fig. 6 Flow visualization of the a) upstroke and b) downstroke (α = 36 deg) of a sinusoidal motion from α = 0–40 deg with k = 0.08 and β = 0 deg.

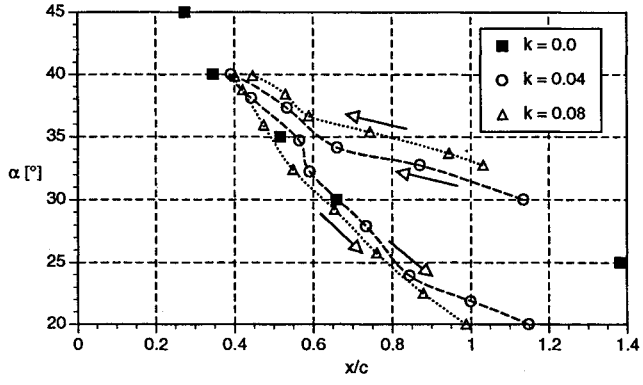

Fig. 7 Effect of varying the reduced frequency on the port strake vortex breakdown location for β = 0 deg.

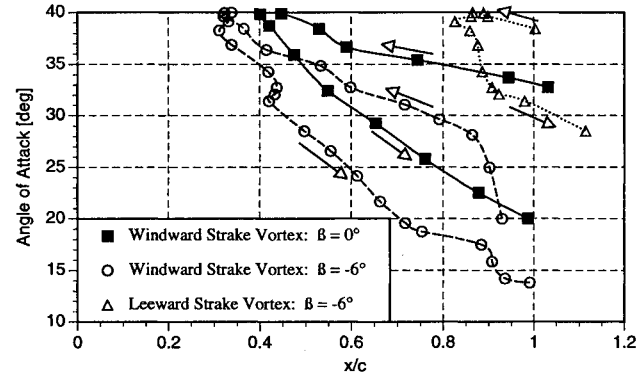

Fig. 8 Sideslip effect on the breakdown locations of the strake vortices during a pitching motion with k = 0.08.

case and two dynamic cases with α = 0–40 deg. This figure illustrates that during the upstroke of the dynamic motion the location of breakdown lags the static position, and that after a sufficient time the location of breakdown lags the static location on the downstroke of the motion. This figure also reveals that for a given α, the axial difference in breakdown location between the upstroke and downstroke grows with increasing reduced frequency. This is also consistent with the findings of studies on delta wings. Similar observations about the lag in vortex breakdown location have been made by several researchers, such as Thompson et al.[19] as well as Brandon[21] for a 70-deg delta wing.

Figure 8 is another graphical presentation of breakdown location of the strake vortices for the model undergoing a dynamic maneuver. This figure shows the effect of sideslip on the dynamic movement of breakdown with angle of attack. All three of these curves show similar differences between the upstroke and downstroke as was just discussed. This figure also shows the overall movement in breakdown position toward the apex for the windward strake vortex, and farther from the apex for the leeward strake vortex for nonzero sideslip. This similar axial movement in the location of breakdown with sideslip was observed for the steady cases as well.

Dynamic force and moment experiments were performed for different reduced frequencies at β = 0, −3, and −6 deg. Figures 9a–9c show the effects of varying the reduced frequency on the normal force coefficient at each sideslip angle. For each sideslip angle the large hysteresis loops have a clockwise sense. There is an overshoot in the normal force coefficient on the upstroke and an undershoot on the downstroke. These hysteresis loops occur at the angles of attack where

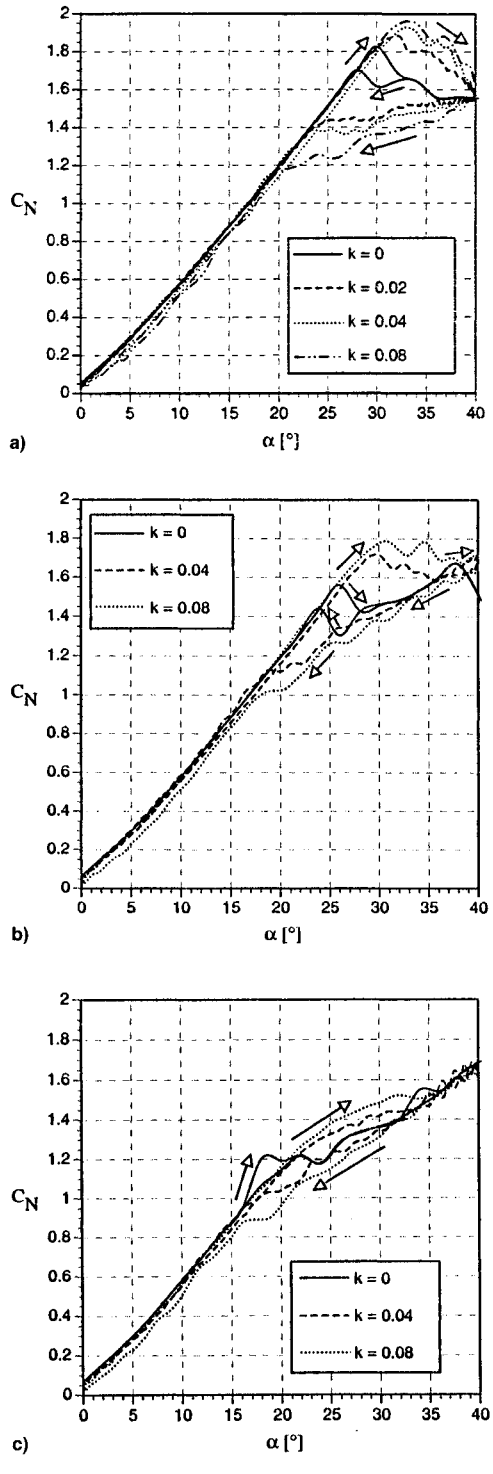

Fig. 9 Effect of varying the reduced frequency on the normal force coefficient at β = a) 0, b) −3, and c) −6 deg.

breakdown is present in the vicinity of the wing. Referring back to Figs. 6a and 6b, for $k = 0.08$ and $\alpha = 36$ deg, breakdown occurred aft of the strake/wing juncture during the upstroke and forward of the strake/wing juncture during the downstroke. Therefore, it would be expected that greater suction would be produced on the upstroke, and hence, a larger normal force, as compared to the downstroke. This behavior is shown in Figs. 9a–9c at each sideslip angle. At a fixed sideslip angle, as the reduced frequency is increased, the size of the hysteresis loop is increased. This trend has been observed in dynamic studies of delta wings. Cunningham and Bushlow[24] have also observed hysteresis loops in the normal force, which increased in size with increasing reduced frequency, for a 76 deg/40 deg/0.53 double delta wing. These figures also reveal that as the magnitude of the sideslip angle is increased, the size of these hysteresis loops, or the area they encircle, decreases. Bragg and Soltani[13] obtained force and moment data for sinusoidal pitching oscillations of a 70-deg delta wing at fixed sideslip angles. They observed hysteresis loops in the aerodynamic coefficients, and they found the size of these loops to decrease as the sideslip angle was increased.

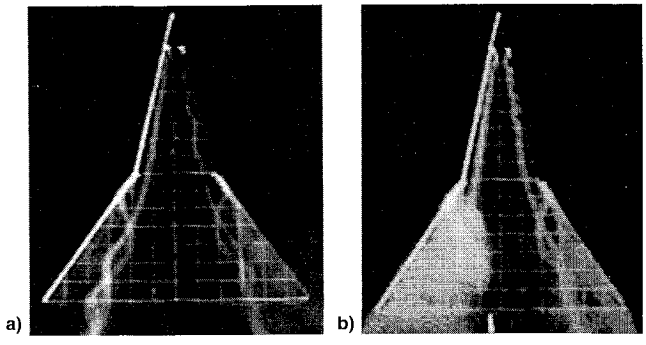

Fig. 10 Static flow visualization images with $\beta = 0$ deg: α = a) 25 and b) 30 deg.

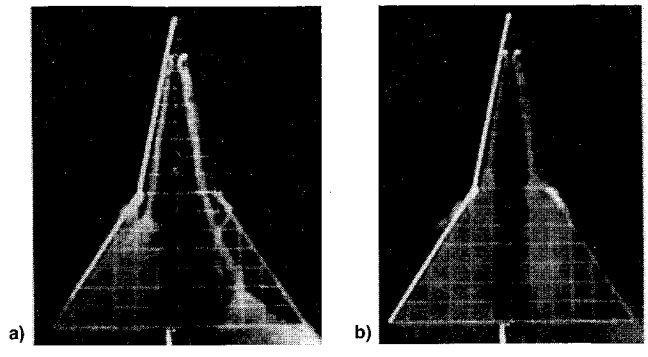

Fig. 11 Dynamic flow visualization images with $k = 0.04$ at $\alpha = 35$ deg and $\beta = 0$ deg: a) upstroke and b) downstroke.

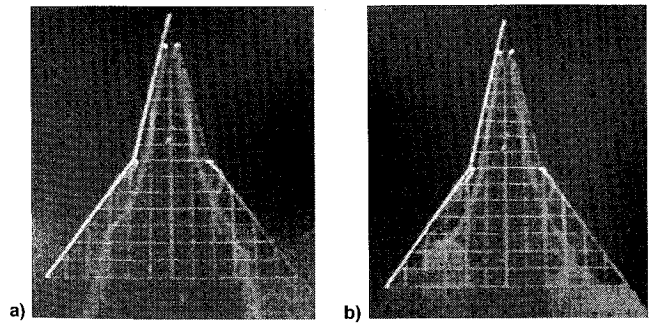

Fig. 12 Dynamic flow visualization images with $k = 0.04$ at $\alpha = 24$ deg and $\beta = 0$ deg: a) upstroke and b) downstroke.

Some significant rolling moment characteristics were observed for the three sideslip angles studied. Figures 10a and 10b, 11a and 11b, and 12a and 12b are planview images from the visualization of the vortex flowfield above the double delta wing at $\beta = 0$ deg. These images are shown to help explain both the static and dynamic rolling moment behavior observed for the double delta wing. These six figures are referenced in Fig. 13a. Figures 13a and 13b demonstrate the rolling moment behavior both statically, with $k = 0$, and dynamically, with $k = 0.04$ and $\alpha = 0$–40 deg, for the double delta planform at $\beta = 0$ and -3 deg, respectively.

At $\beta = 0$ deg a large negative rolling moment was observed for the static case in the approximate region 28 deg $< \alpha <$ 36 deg. Figure 10a displays the vortex flowfield above the double delta wing at $\beta = 0$ deg and $\alpha = 25$ deg for static conditions. This image shows that at $\alpha = 25$ deg neither the strake nor wing vortices break down in the vicinity of the wing. However, at $\alpha = 30$ deg, Fig. 10b reveals a highly asymmetric flowfield. From this figure it is difficult to determine the breakdown location of the wing vortices, but it appears that the starboard wing vortex exists without breakdown occurring over at least most of the main wing. The port wing vortex appears to be breaking down nearer to the strake/wing juncture. The breakdown location of the strake vortices is marked well by the smoke. On the port side of the wing breakdown of the strake vortex is occurring just aft of the strake/wing juncture. On the starboard side of the wing the strake vortex does not experience breakdown above the wing surface. Therefore, a large asymmetry in the location of vortex breakdown is observed at $\alpha = 30$ deg.

In a previous study[11] of this wing, under static conditions, the heights of the strake vortex cores above the surface of the wing were found to be symmetric between the port and starboard sides at $\beta = 0$. Given this symmetry at $\beta = 0$, since breakdown does not occur above the wing for the starboard strake vortex, and it occurs near the strake/wing juncture for the port strake vortex, the starboard side of the wing would experience a larger suction than the port side. This would yield a strong negative rolling moment as shown in Fig. 13a.

Figure 13a also shows the rolling moment behavior for the wing undergoing a pitching motion. Compared to the static case, a negative rolling moment is observed during the upstroke of the motion at a higher angle of attack, for 33 deg $< \alpha <$ 40 deg. Figures 11a and 11b show the flowfield above the double delta wing during the upstroke and downstroke of the same pitching motion at $\alpha = 35$ deg. During the upstroke, Fig. 11a displays a sizable asymmetry in the breakdown location of the strake vortices. The port strake vortex breakdown location is just aft of the strake/wing juncture, and the location of breakdown for the starboard strake vortex is just upstream of the trailing edge. This asymmetry would also produce an imbalance in suction between the port and starboard sides of the wing yielding a negative rolling moment. The axial difference in the location of strake vortex breakdown between the port and starboard sides, and therefore, the magnitude of the negative rolling moment observed over this region during the upstroke, is not as large as that observed for the static case at $\alpha = 30$ deg. During the downstroke, Fig. 11b shows that breakdown for the strake vortices is highly symmetric and occurs near the strake/wing junctures. This symmetry does not generate a significant rolling moment as shown in Fig. 13a.

Figures 12a and 12b illustrate the vortex flowfield above the double delta wing during the upstroke and downstroke at $\alpha = 24$ deg. During the upstroke, breakdown is not observed on either side of the wing, as shown in Fig. 12a; and no significant rolling moment is generated, as shown in Fig. 13a. However, the double delta wing experiences a small region of negative rolling moment during the downstroke for lower angles of attack, 23 deg $< \alpha <$ 27 deg, than for the static case. Figure 12b reveals a smaller asymmetry in breakdown

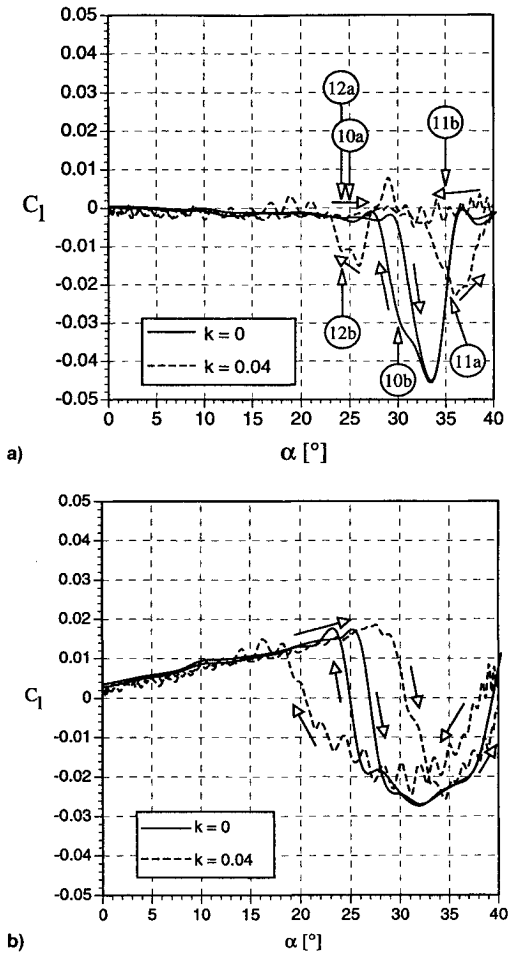

Fig. 13 Comparison of the static and dynamic rolling moment coefficient at β = a) 0 and b) −3 deg.

location at $\alpha = 24$ deg, and therefore, a smaller negative rolling moment for the downstroke than what was observed during the upstroke at $\alpha = 35$ deg.

The lag in the position of vortex breakdown, which was discussed earlier, is demonstrated again in the flow visualization images. Figure 13a illustrates the lag in the flowfield response for a dynamic case over the static case. During the upstroke, the region of negative rolling moment, although not as large in magnitude with the static case, is delayed to higher angles of attack. During the downstroke, the region of negative rolling moment, again not as large in magnitude, is delayed to lower angles of attack. Although not illustrated in Fig. 13a, as the reduced frequency was increased from 0.0 through 0.08, the lag increased, both on the upstroke and the downstroke. This trend is consistent with previous findings for delta wings.

Figure 13b shows the rolling moment coefficient for $k = 0$ and 0.04 at $\beta = -3$ deg. The rolling moment for the static case was discussed previously. This figure illustrates that when the double delta wing is driven dynamically, the size of the clockwise dynamic rolling moment hysteresis loop is larger than the size of the static hysteresis loop, which can be explained by the lag in the vortex breakdown response for the dynamic case over the static case. Although not shown, the size of both the static and dynamic rolling moment hysteresis loops decreased from $\beta = -3$ deg to $\beta = -6$ deg.

Effect of Varying the Angle-of-Attack Range

For $k = 0.04$ the angle-of-attack range of the motions was varied. Figure 14, showing C_N at $\beta = 0$ deg, illustrates that for the same reduced frequency the largest hysteresis loops

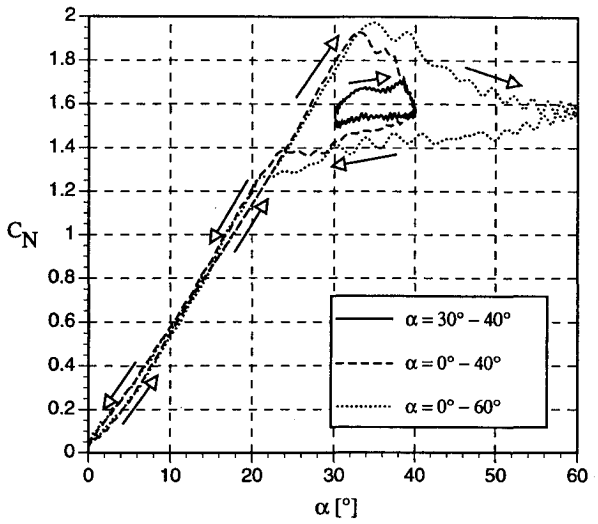

Fig. 14 Effect of varying the angle-of-attack range on the normal force coefficient with $k = 0.04$ at $\beta = 0$ deg.

are created by the largest angle-of-attack ranges. For the same reduced frequency, a larger α range means that the model must be driven at higher angular velocities to cover the larger α range in the same time period as for the smaller α range. For a fixed α range, higher angular velocities would translate into higher pitching frequencies, and therefore, higher reduced frequencies. As just discussed in the previous section, higher reduced frequencies increase the size of the aerodynamic hysteresis loops. Therefore, it might be expected that a larger α range would create a larger hysteresis for the same reduced frequency. These figures also show that the values of C_N are nearly the same at the lower angles of attack. Also, the values for C_N near $\alpha = 40$ deg are very similar for motions with that as the maximum angle of attack. The largest differences between the upstroke and the downstroke are observed around α_{stall}.

Figure 15 shows the rolling moment coefficient for three angle-of-attack ranges at $\beta = 0$ deg. Note that only the data for the range in angle of attack from 30 deg $\leq \alpha \leq$ 40 deg is shown. Over this angle-of-attack range, the hysteresis loops are seen to decrease in size with increasing pitching range. As was discussed for the normal force behavior with increasing angle-of-attack range at a fixed reduced frequency, the angular velocity through which the model is driven must increase. The previous discussion of the rolling moment behavior pointed out that with increasing reduced frequency, the magnitude of the negative rolling moment found during the upstroke, over this angle-of-attack range, decreased. Similarly, increasing the angle-of-attack range for a fixed reduced frequency decreased the magnitude of the roll moment during the upstroke at the higher angles of attack. Figure 15 also reveals small oscillations in the roll moment with a frequency of 21 Hz. This frequency, when put in nondimensional form and compared to the reduced wing-rock frequency of 0.06 found by Arena[25] for an 80-deg delta, yielded a value of 0.35. Therefore, these oscillations do not appear to be due to a tendency to wing rock, but more testing, such as free-to-roll experiments, would be needed to determine if this planform could produce a wing-rock motion under the appropriate conditions. The natural frequency of the balance in torsion was determined to be 21 Hz, which accounts for the 21-Hz frequency component found in the roll moment data. It should be noted that since the roll moment data was an ensemble average of data obtained over 60 cycles of motion, these oscillations were repeatable. Varying the number of cycles used in the ensemble averaging, from 30 to 60, yielded no discernible difference in the magnitude of these oscillations.

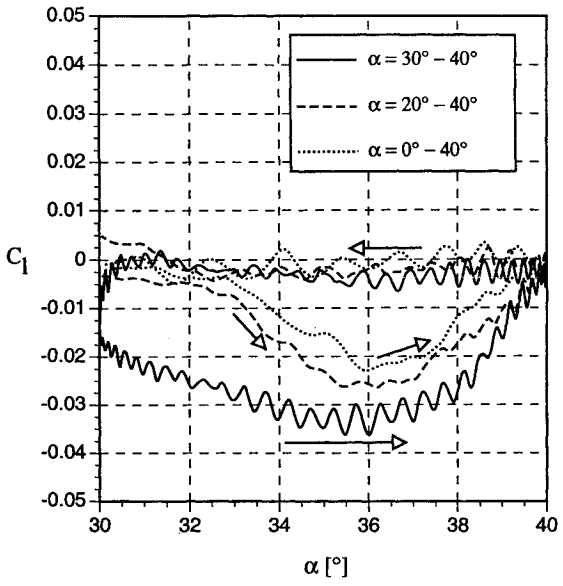

Fig. 15 Effect of varying the angle-of-attack range on the rolling moment coefficient with $k = 0.04$ at $\beta = 0$ deg. (Note only 30 deg $\leq \alpha \leq$ 40 deg is shown.)

Therefore, the aerodynamics must be locking the roll moment behavior into this repeatable mode.

Conclusions

The following are some general observations that were made, from flow visualization and force, and moment experiments, about the static and dynamic aerodynamics of an 80 deg/60 deg/0.6 double delta wing for angle-of-attack variations with and without sideslip.

1) The back horizontal bar of the yoke-type pitching mechanism was not found to cause any significant static or dynamic interference effects with the double-delta-wing flowfield.

2) A clockwise static hysteresis was observed in both the normal force and rolling moment coefficients at sideslip angles of $\beta = 0$, -3, and -6 deg. An increase in the magnitude of sideslip was found to lower the angle of attack at which the hysteresis occurred. For these relatively small sideslip angles, the model exhibited static roll stability for lower angles of attack, but for higher angles of attack significant negative roll moments were generated at each sideslip angle. The largest roll moment magnitude was generated at $\beta = 0$ deg.

3) The model was driven through sinusoidal pitching motions of varying reduced frequency over the same angle-of-attack range. The location of breakdown for the strake vortices during an upstroke was found to be farther from the apex than during the downstroke of the same motion. This disparity in the distance between the upstroke and downstroke breakdown location was seen to increase with increasing reduced frequency. This increase in the breakdown location disparity caused an increase in the size of the hysteresis loops observed for the normal force and rolling moment. For zero sideslip, an increase in the reduced frequency also decreased the magnitude of the roll moment.

4) The model was also driven through sinusoidal pitching motions of varying angle-of-attack range with a fixed reduced frequency. Larger angle-of-attack ranges resulted in higher angular pitch rates, which yielded larger hysteresis loops in the normal force coefficient. The size of these hysteresis loops decreased not only with decreasing angle-of-attack range, but also with increasing magnitudes of the sideslip angle. For the roll moment, an increase in the angle-of-attack range decreased the magnitude of the roll moment at the higher angles of attack.

Acknowledgments

The authors wish to acknowledge the technical and financial support provided by Wayne Ely at the McDonnell Aircraft Company, and his co-workers for providing the force balance. This research was conducted in the Hessert Center for Aerospace Research at the University of Notre Dame. The authors also wish to acknowledge the support of Michael Swadener and Joel Preston of the Department of Aerospace and Mechanical Engineering for constructing the model and test section, and for assisting with the data acquisition systems, respectively. Acknowledgment is also given to Andrew Arena Jr. of Oklahoma State University for sharing his knowledge about the motion control system that he developed at the University of Notre Dame. Mention is also given to Matthew Grismer for his assistance during some of the flow visualization experiments.

References

[1]Wentz, W. H., Jr., and McMahon, M. C., "An Experimental Investigation of the Flow Fields About Delta and Double-Delta Wings at Low Speeds," NASA CR-521, Aug. 1966.

[2]Wentz, W. H., Jr., and McMahon, M. C., "Further Experimental Investigations of Delta and Double-Delta Wing Flow Fields at Low Speeds," NASA CR-714, Feb. 1967.

[3]Brennenstuhl, U., and Hummel, D., "Vortex Formation over Double-Delta Wings," International Council of the Aeronautical Sciences, ICAS-82-6.6.3, Germany, 1982.

[4]Olsen, P. E., and Nelson, R. C., "Vortex Interaction over Double Delta Wings at High Angles of Attack," AIAA Paper 89-2191, July 1989.

[5]Graves, T. V., Nelson, R. C., Schwimley, S. L., and Ely, W. L., "Aerodynamic Performance of Strake Wing Configurations," *NASA High-Angle-of-Attack Technology Conference*, NASA CP-3149, 1990, pp. 173–204.

[6]Maseland, J. E. J., and Verhaagen, N. G., "Experimental and Numerical Investigation of Vortex Flow over a 76/60-Deg Double-Delta Wing," LR-680 Rept., Delft Univ. of Technology, The Netherlands, April 1992.

[7]Hummel, D., "Aerodynamic Investigations on Double-Delta-Wings in Unsymmetrical Flow," 87-2, BMVg-FBWT, Forschungsbericht Aus Der Wehrtechnik, Dec. 1986.

[8]Manor, D., and Wentz, W. H., Jr., "Flow over Double-Delta Wing and Wing Body at High α," *Journal of Aircraft*, Vol. 22, No. 1, 1985, pp. 78–82.

[9]Verhaagen, N. G., "Some Low-Speed Wind-Tunnel Experiments on a Sharp-Edged Delta Wing of Aspect Ratio 1, with and Without Yaw," LR-283 Rept., Delft Univ. of Technology, The Netherlands, Aug. 1979.

[10]Verhaagen, N. G., and Naarding, S. H. J., "Experimental and Numerical Investigation of Vortex Flow over a Sideslipping Delta Wing," *Journal of Aircraft*, Vol. 26, No. 11, 1989, pp. 971–978.

[11]Grismer, D. S., Nelson, R. C., and Ely, W. L., "The Aerodynamic Effects of Sideslip on Double Delta Wings," AIAA Paper 93-0053, Jan. 1993.

[12]Grismer, D. S., Nelson, R. C., and Ely, W. L., "An Experimental Study of Double Delta Wings in Sideslip," AIAA Paper 91-3308, Sept. 1991.

[13]Bragg, M. B., and Soltani, M. R., "An Experimental Study of the Effect of Asymmetrical Vortex Bursting on a Pitching Delta Wing," AIAA Paper 88-4334, Aug. 1988.

[14]Bragg, M. B., and Soltani, M. R., "Measured Forces and Moments on a Delta Wing During Pitch-Up," *Journal of Aircraft*, Vol. 27, No. 3, 1990, pp. 262–267.

[15]Brandon, J. M., and Shah, G. H., "Effect of Large Amplitude Pitching Motions on the Unsteady Aerodynamic Characteristics of Flat-Plate Wings," *Proceedings of the AIAA Atmospheric Flight Mechanics Conference*, AIAA, Washington, DC, 1988, pp. 35–45.

[16]Jarrah, M.-A. M., "Low-Speed Wind-Tunnel Investigation of Flow About Delta Wings, Oscillating in Pitch to Very High Angle of Attack," AIAA Paper 89-0295, Jan. 1989.

[17]Thompson, S. A., "The Unsteady Aerodynamics of a Delta Wing Undergoing Large Amplitude Pitching Motions," Ph.D. Dissertation, Univ. of Notre Dame, Notre Dame, IN, April 1992.

[18]Thompson, S. A., Batill, S. M., and Nelson, R. C., "Delta Wing Surface Pressures for High Angle of Attack Maneuvers," *Proceedings*

dingsof the AIAA Atmospheric Flight Mechanics Conference, AIAA, Washington, DC, 1990, pp. 184–193.

[19]Thompson, S. A., Batill, S. M., and Nelson, R. C., "Separated Flowfield on a Slender Wing Undergoing Transient Pitching Motions," *Journal of Aircraft*, Vol. 28, No. 8, 1991, pp. 489–495.

[20]Soltani, M. R., Bragg, M. B., and Brandon, J. M., "Measurements on an Oscillating 70-Deg Delta Wing in Subsonic Flow," *Journal of Aircraft*, Vol. 27, No. 3, 1990, pp. 211–217.

[21]Brandon, J. M., "Dynamic Stall Effects and Applications to High Performance Aircraft," AGARD-R-776, NASA Langley Research Center, Hampton, VA, 1991.

[22]Cunningham, A. M., Jr., and Den Boer, R. G., "Harmonic Analysis of Force and Pressure Data Results for an Oscillating Straked Wing at High Angles," AIAA Paper 87-2494, Aug. 1987.

[23]Cunningham, A. M., Jr., "Unsteady Low-Speed Windtunnel Test of a Straked Delta Wing, Oscillating in Pitch—Parts I–VI," Air Force Wright Aeronautical Labs., AFWAL-TR-87-3098, April 1988.

[24]Cunningham, A. M., Jr., and Bushlow, T., "Steady and Unsteady Force Testing of Fighter Aircraft Models in a Water Tunnel," *Proceedings of the AIAA Atmospheric Flight Mechanics Conference*, AIAA, Washington, DC, 1990, pp. 222–237.

[25]Arena, A. S., Jr., "An Experimental and Computational Investigation of Slender Wings Undergoing Wing Rock," Ph.D. Dissertation, Univ. of Notre Dame, Notre Dame, IN, April 1992.

[26]Jarrah, M.-A. M., "Unsteady Aerodynamics of Delta Wings Performing Maneuvers to High Angle of Attack," Ph.D. Dissertation, Stanford Univ., Stanford, CA, Dec. 1988.

[27]Visser, K. D., Nelson, R. C., and Ng, T. T., "Method of Cold Smoke Generation for Vortex Core Tagging," *Journal of Aircraft*, Vol. 25, No. 11, 1988, pp. 1069–1071.

[28]Thompson, D. H., "A Visualisation Study of the Vortex Flow Around Double-Delta Wings," Aeronautical Research Labs., ARL-AERO-R-165, Aug. 1985.

[29]O'Neil, P. J., Roos, F. W., Kegelman, J. T., Barnett, R. M., and Hawk, J. D., "Investigation of Flow Characteristics of a Developed Vortex," Naval Air Development Center, NADC-89114-60, May 1989.

[30]Pass, C. Q., "A Wake Blockage Correction Method for Small Subsonic Wind Tunnels," AIAA Paper 87-0294, Jan. 1987.

[31]Maskell, E. C., "A Theory of the Blockage Effects on Bluff Bodies and Stalled Wings in a Closed Wind Tunnel," Aeronautical Research Council, R&M 3400, Nov. 1963.

[32]Garner, H. C., Rogers, E. W. E., Acum, W. E. A., and Maskell, E. C., "Subsonic Wind Tunnel Wall Corrections," AGARDograph 109, Oct. 1966.

[33]Manor, D., and Wentz, W. H., Jr., "Experimental Investigation of Vortex Flow over Double-Delta Wing at High α," *Israel Journal of Technology*, Vol. 23, 1986/1987, pp. 57–63.